Nuclear Inst, and Methods in Physics Research B 422 (2018) 18–23

Contents lists available at ScienceDirect

Nuclear Inst. and Methods in Physics Research B

journal homepage: www.elsevier.com/locate/nimb

Relativistic effects in the energy loss of a fast charged particle moving parallel to a two-dimensional electron gas

Zoran L. Mišković[a,*], Kamran Akbari[b], Silvina Segui[c,1], Juana L. Gervasoni[d,2], Néstor R. Arista[d]

[a] Department of Applied Mathematics, and Waterloo Institute for Nanotechnology, University of Waterloo, Waterloo, Ontario N2L 3G1, Canada
[b] Department of Applied Mathematics, University of Waterloo, Waterloo, Ontario N2L 3G1, Canada
[c] Centro Atómico Bariloche, Comisión Nacional de Energía Atómica, Av. Bustillo 9500, 8400 S.C. de Bariloche, Argentina
[d] Instituto Balseiro, Universidad Nacional de Cuyo and Centro Atómico Bariloche, Comisión Nacional de Energía Atómica, Av. Bustillo 9500, 8400 S.C. de Bariloche, Argentina

ARTICLE INFO

Keywords:
Relativistic effects
Stopping power
Plasmon excitation
Graphene
Two-dimensional electron gas

ABSTRACT

We present a fully relativistic formulation for the energy loss rate of a charged particle moving parallel to a sheet containing two-dimensional electron gas, allowing that its in-plane polarization may be described by different longitudinal and transverse conductivities. We apply our formulation to the case of a doped graphene layer in the terahertz range of frequencies, where excitation of the Dirac plasmon polariton (DPP) in graphene plays a major role. By using the Drude model with zero damping we evaluate the energy loss rate due to excitation of the DPP, and show that the retardation effects are important when the incident particle speed and its distance from graphene both increase. Interestingly, the retarded energy loss rate obtained in this manner may be both larger and smaller than its non-retarded counterpart for different combinations of the particle speed and distance.

1. Introduction

Developments in the area of Nanophotonics and Optoloectronic devices, which are based on two-dimensional (2D) materials, exploit several favorable optical properties of graphene [1]. In particular, applications in the frequency range from terahertz (THz) to the infrared (IR) make use of the so-called Dirac plasmon (or sheet plasmon), which arises from low-energy intraband excitations within the π electron bands in doped graphene [2]. In that context, it was shown that the dispersion relation of the Dirac plasmon can be easily tuned by changing the chemical potential in graphene via external gates, whereas the corresponding plasmon polariton exhibits long propagation distances along graphene and strong confinement of the associated electric field in directions perpendicular to graphene [3].

In recent years there has been an increase of interest in using electron beams to generate radiation from graphene in the THz range of frequencies using different electron trajectories, including both aloof scattering [4,5] and normal incidence [6]. It has been shown that, when the incident charged particle moves parallel to graphene, its velocity may be used as additional tuning parameter, besides the chemical potential in graphene, for creating radiation at various frequencies [4,5]. Being interested in the THz frequencies, those authors adopted a model for dynamic polarization of doped graphene based on the Drude model [4–6], which was also found to be reliable in many other applications of graphene in the area of Nanoplasmonics [1,7].

In our previous work, we have studied stopping power and image force on charged particles moving parallel to graphene using a non-relativistic approach to elucidate the role of Dirac plasmon in doped graphene [8,9]. More recently, we have developed a fully relativistic treatment of the energy loss and induced transition radiation from graphene traversed by a fast charged particle under normal incidence, and applied it to single [10] and multiple graphene layers [11].

In this work we adapt our relativistic treatment of Refs. [10,11] to the case of a charged particle moving parallel to a single layer of doped graphene. When the particle moves with constant speed in the absence of other polarizable media, no radiation is generated from graphene, whereas its energy loss to the electron excitations in graphene occurs at a constant rate, which is related to the usual stopping power for a parallel incidence trajectory [8,9]. The study of relativistic effects in stopping power of charged particles has a long history, mostly focusing on solid targets (see, e.g., Ref. [12] and references therein) and their surfaces [13,14], whereas relatively less is known for strictly 2D targets. In that respect, we note that our formulation of the energy loss rate for incident particle is given in terms of the 2D conductivity of the target

* Corresponding author.
E-mail address: zmiskovi@uwaterloo.ca (Z.L. Mišković).
[1] Consejo Nacional de Investigaciones Cientí ficas y Técnicas of Argentina (CONICET).
[2] Consejo Nacional de Investigaciones Cientí ficas y Técnicas of Argentina (CONICET).

https://doi.org/10.1016/j.nimb.2018.02.025
Received 30 September 2017; Received in revised form 16 February 2018; Accepted 21 February 2018

and hence it may be applied to any 2D material, not just graphene.

The main novelty regarding our description of graphene in comparison with Refs. [10,11] is that, in the case of parallel trajectory of the incident particle, graphene may exhibit differences between its longitudinal and transverse polarizations. Accordingly, our formulation of the problem in this work is more general, allowing for a tensorial in-plane conductivity of graphene. However, since we are primarily interested in the processes occurring in graphene at the THz to mid-IR range of frequencies, it is safe to take the long wavelength limit of the graphene's conductivity [15]. In that limit, the longitudinal and transverse conductivities become equal, and are well described by a sum of the Drude model describing the intraband electron transitions and a term, which describes interband transitions between graphene's π electron bands [16–18]. Moreover, focusing on the role of Dirac plasmon in doped graphene at the THz frequencies, it turns out that using just the Drude term for graphene conductivity suffices [1,4–7].

While it was shown in our previous work that the damping factor in the Drude model exerts rather strong effects on energy losses of the perpendicularly incident charged particle due to the excitations of charge carriers in graphene [10], taking the limit of zero damping can provide an insight into the efficiency of exciting the collective mode in graphene known as the Dirac plasmon polariton (DPP) [11]. Accordingly, taking the limit of zero damping in this work will enable us to evaluate the energy loss rate due to the excitation of the long-lived DPP in doped graphene as a function of the incident particle speed and its distance from graphene.

After outlining a general theoretical formulation, we present and discuss several results for the energy loss rate based on the Drude model with zero damping, which are followed by our concluding remarks. Note that, unless otherwise explicitly stated, we use Gaussian units of Electrodynamics [19].

2. Theory

We consider an infinitely large conducting layer of zero thickness, placed in vacuum, which occupies the $z = 0$ plane of a three-dimensional (3D) Cartesian system with coordinates $\mathbf{R} = \{x,y,z\}$, and assume that a point charge Ze moves with constant velocity $\mathbf{v}$ parallel to that layer at a fixed distance b. Since both the external charge and the induced charge in the layer are moving uniformly, no electromagnetic radiation is expected in the absence of dielectric environment. We assume that the conducting layer is isotropic in the direction of the in-plane coordinates $\mathbf{r} = \{x,y\}$, but the polarization of its electron gas may depend on the direction of propagation relative to the in-plane wavevectors $\mathbf{k} = \{k_x,k_y\}$. This property is generally captured by a tensorial in-plane conductivity of the layer that depends on $k = \sqrt{k_x^2 + k_y^2}$ and frequency ω, but may exhibit distinct longitudinal and transverse components, $\sigma_l(k,\omega)$ and $\sigma_t(k,\omega)$, which describe different responses of the electron gas in the directions of the unit vectors $\hat{\mathbf{k}}$ and $\hat{\boldsymbol{\tau}} = \hat{\mathbf{z}} \times \hat{\mathbf{k}}$, respectively. Accordingly, we shall also define the longitudinal and transverse components of the external particle's velocity via $\mathbf{v} = \hat{\mathbf{k}}v_l + \hat{\boldsymbol{\tau}}v_t$.

As in Ref. [10], we use the Hertz vector $\boldsymbol{\Pi}(\mathbf{R},t)$ [20] and perform Fourier transforms with respect to the in-plane coordinates and time, according to

$$\boldsymbol{\Pi}(\mathbf{k},z,\omega) = \iint d^2\mathbf{r}\, e^{-i\mathbf{k}\cdot\mathbf{r}} \int_{-\infty}^{\infty} dt\, e^{i\omega t}\boldsymbol{\Pi}(\mathbf{R},t), \tag{1}$$

which enables us to express the corresponding electric field as

$$\mathbf{E}(\mathbf{k},z,\omega) = \frac{\omega^2}{c^2}[\boldsymbol{\Pi}_{\parallel}(\mathbf{k},z,\omega) + \hat{\mathbf{z}}\Pi_z(\mathbf{k},z,\omega)] + \left(i\mathbf{k} + \hat{\mathbf{z}}\frac{\partial}{\partial z}\right)\left[i\mathbf{k}\cdot\boldsymbol{\Pi}_{\parallel}(\mathbf{k},z,\omega) + \frac{\partial}{\partial z}\Pi_z(\mathbf{k},z,\omega)\right], \tag{2}$$

where $\boldsymbol{\Pi}_{\parallel}(\mathbf{k},z,\omega)$ and $\Pi_z(\mathbf{k},z,\omega)$ are components of the Hertz vector parallel and perpendicular to the conducting layer, and c is the speed of light in vacuum. The advantage of using the Hertz vector is that it may be expressed in terms of the source charge current, $\mathbf{J}(\mathbf{k},z,\omega)$, by means of a free-space, retarded Green's function, $G(k,z,\omega)$, for a non-homogeneous Helmholtz equation in scalar form as [10]

$$\boldsymbol{\Pi}(\mathbf{k},z,\omega) = \frac{i}{\omega}\int_{-\infty}^{\infty} dz'\, G(k,z-z',\omega)\mathbf{J}(\mathbf{k},z',\omega), \tag{3}$$

where

$$G(k,z,\omega) = \frac{2\pi}{\alpha(k,\omega)}e^{-|z|\alpha(k,\omega)} \tag{4}$$

with

$$\alpha(k,\omega) = \sqrt{k^2 - \left(\frac{\omega}{c}\right)^2}, \tag{5}$$

for $|\omega| < ck$.

Note that the current density of the moving external charge may be written as

$$\mathbf{J}_{\rm ext}(\mathbf{R},t) = \mathbf{v}\rho_{\rm ext}^{\rm cm}(\mathbf{r}-\mathbf{v}t,z), \tag{6}$$

where $\rho_{\rm ext}^{\rm cm}(\mathbf{r},z) = Ze\delta(\mathbf{r})\delta(z-b)$ is the density of a point charge in its center-of-mass (cm) frame of reference. Performing the Fourier transform, we obtain

$$\mathbf{J}_{\rm ext}(\mathbf{k},z,\omega) = 2\pi Ze\mathbf{v}\delta(\omega-\mathbf{k}\cdot\mathbf{v})\delta(z-b), \tag{7}$$

which gives the corresponding Hertz vector from Eq. (3) in the form

$$\boldsymbol{\Pi}_{\rm ext}(\mathbf{k},z,\omega) = \frac{i}{\omega}G(k,z-b,\omega)2\pi Ze\mathbf{v}\delta(\omega-\mathbf{k}\cdot\mathbf{v}). \tag{8}$$

Clearly, the Dirac's delta function in Eq. (8) only selects frequencies $\omega = \mathbf{k}\cdot\mathbf{v} = kv_l$, corresponding to a resonance condition for exciting the polarization modes in the conducting layer, which lie outside the light cone, $|\omega| < ck$. While using Eq. (8) in Eq. (2) gives an electric field due to the external charge that has all three non-zero Cartesian components, we only require its components parallel to the conducting layer, which may be conveniently decomposed into the longitudinal and transverse parts via $\mathbf{E}_{\rm ext}^{\parallel} = \hat{\mathbf{k}}E_{\rm ext}^{(l)} + \hat{\boldsymbol{\tau}}E_{\rm ext}^{(t)}$, where

$$E_{\rm ext}^{(l)}(\mathbf{k},z,\omega) = \left(\frac{\omega^2}{c^2} - k^2\right)\frac{i}{\omega}G(k,z-b,\omega)2\pi Zev_l\delta(\omega-\mathbf{k}\cdot\mathbf{v}), \tag{9}$$

$$E_{\rm ext}^{(t)}(\mathbf{k},z,\omega) = \frac{\omega^2}{c^2}\frac{i}{\omega}G(k,z-b,\omega)2\pi Zev_t\delta(\omega-\mathbf{k}\cdot\mathbf{v}). \tag{10}$$

On the other hand, the induced charge carrier current density in the conducting layer may be written as

$$\mathbf{J}_{\rm ind}(\mathbf{k},z,\omega) = \delta(z)\mathbf{j}(\mathbf{k},\omega), \tag{11}$$

where the in-plane current density may be expressed in terms of a generalized Ohm's law as $\mathbf{j}(\mathbf{k},\omega) = \underline{\sigma}(k,\omega)\mathbf{E}_{\rm tot}^{\parallel}(\mathbf{k},0,\omega)$,with $\underline{\sigma} = {\rm diag}[\sigma_l,\sigma_t]$ being a conductivity tensor in diagonal form and $\mathbf{E}_{\rm tot}^{\parallel}(\mathbf{k},0,\omega)$ the in-plane (tangential) component of the total electric field evaluated at the plane $z = 0$. Using Eq. (11) in Eq. (3) gives the Hertz vector due to the induced currents in the form

$$bfPi_{\rm ind}(\mathbf{k},z,\omega) = \frac{i}{\omega}G(k,z,\omega)\,\underline{\sigma}(k,\omega)\mathbf{E}_{\rm tot}^{\parallel}(\mathbf{k},0,\omega), \tag{12}$$

which when used in Eq. (2) yields all three Cartesian components of the corresponding electric field. However, we only require components of the induced electric field that are parallel to the conducing layer, which are again decomposed into the longitudinal and transverse parts via $\mathbf{E}_{\rm ind}^{\parallel} = \hat{\mathbf{k}}E_{\rm ind}^{(l)} + \hat{\boldsymbol{\tau}}E_{\rm ind}^{(t)}$, where

$$E_{\rm ind}^{(l)}(\mathbf{k},z,\omega) = \left(\frac{\omega^2}{c^2} - k^2\right)\frac{i}{\omega}G(k,z,\omega)\sigma_l(k,\omega)E_{\rm tot}^{(l)}(\mathbf{k},0,\omega) \tag{13}$$

$$E_{\rm ind}^{(t)}(\mathbf{k},z,\omega) = \frac{\omega^2}{c^2}\frac{i}{\omega}G(k,z,\omega)\sigma_t(k,\omega)E_{\rm tot}^{(t)}(\mathbf{k},0,\omega). \tag{14}$$

In order to obtain a self-consistent set of equations for the

longitudinal and transverse components of the total in-plane electric filed, $E^{(l,t)}_{\rm tot}(\mathbf{k},0,\omega) = E^{(l,t)}_{\rm ext}(\mathbf{k},0,\omega) + E^{(l,t)}_{\rm ind}(\mathbf{k},0,\omega)$, we set $z = 0$ in Eqs. (9), (10), (13), and (14), whence adding Eqs. (9) and (13) and solving the resulting equation gives

$$E^{(l)}_{\rm tot}(\mathbf{k},0,\omega) = \frac{\left(\frac{\omega^2}{c^2}-k^2\right)\frac{i}{\omega}G(k,b,\omega)}{1-\left(\frac{\omega^2}{c^2}-k^2\right)\frac{i}{\omega}G(k,0,\omega)\sigma_l(k,\omega)}2\pi Ze v_l\delta(\omega-\mathbf{k}\cdot\mathbf{v}), \tag{15}$$

whereas adding Eqs. (10) and (14) and solving the resulting equation gives

$$E^{(t)}_{\rm tot}(\mathbf{k},0,\omega) = \frac{\frac{\omega^2}{c^2}\frac{i}{\omega}G(k,b,\omega)}{1-\frac{\omega^2}{c^2}\frac{i}{\omega}G(k,0,\omega)\sigma_t(k,\omega)}2\pi Ze v_t\delta(\omega-\mathbf{k}\cdot\mathbf{v}). \tag{16}$$

Using the results obtained in Eqs. (15) and (16) in the right hand sides of Eqs. (13) and (14) gives final expressions for the longitudinal and transverse components of the induced electric fields at arbitrary position z, respectively.

Notice that the thus obtained expressions for $E^{(l,t)}_{\rm ind}(\mathbf{k},z,\omega)$ contain a delta function $\delta(\omega-\mathbf{k}\cdot\mathbf{v})$, which is "inherited" from the external current density in Eq. (7). Thus, performing the inverse Fourier transform shows that the induced electric field is stationary in the moving frame of reference attached to the external particle, so that the spatiotemporal dependence of its parallel component may be written as $\mathbf{E}^{\parallel}_{\rm ind}(\mathbf{R},t) = \mathbf{E}^{\rm cm,\parallel}_{\rm ind}(\mathbf{r}-\mathbf{v}t,z)$. Here, the induced electric field parallel to the conducting layer is defined in the center-of-mass (cm) frame via its 2D spatial Fourier transform as

$$\mathbf{E}^{\rm cm,\parallel}_{\rm ind}(\mathbf{k},z) = -2\pi i Ze\,{\rm e}^{-(|z|+|b|)\alpha(k,kv_l)}\times\left\{\hat{\mathbf{k}}\frac{\alpha(k,kv_l)}{k}\left[\frac{1}{\epsilon_l(k,kv_l)}-1\right]\right.$$
$$\left.-\hat{\boldsymbol{\tau}}\frac{v_l v_t}{c^2}\frac{k}{\alpha(k,kv_l)}\left[\frac{1}{\epsilon_t(k,kv_l)}-1\right]\right\}, \tag{17}$$

where we have taken into account that $\omega = \mathbf{k}\cdot\mathbf{v} = kv_l$, and we defined the longitudinal and transverse dielectric functions of the conducting layer by

$$\epsilon_l(k,\omega) = 1 + 2\pi i\frac{\alpha(k,\omega)}{\omega}\sigma_l(k,\omega), \tag{18}$$

$$\epsilon_t(k,\omega) = 1-2\pi i\frac{\omega}{c^2\alpha(k,\omega)}\sigma_t(k,\omega), \tag{19}$$

respectively.

One may further refer to Eq. (6) and write the rate of energy dissipation in the conducting layer as

$$\frac{dW}{dt} = -\iiint d^3\mathbf{R}\mathbf{J}_{\rm ext}(\mathbf{R},t)\cdot\mathbf{E}_{\rm ind}(\mathbf{R},t) = -\iint d^2\mathbf{r}\int dz\,\rho^{\rm cm}_{\rm ext}(\mathbf{r}-\mathbf{v}t,z)\mathbf{v}\cdot$$
$$\mathbf{E}^{\rm cm,\parallel}_{\rm ind}(\mathbf{r}-\mathbf{v}t,z) = -\iint d^2\mathbf{r}\int dz\,\rho^{\rm cm}_{\rm ext}(\mathbf{r},z)\mathbf{v}\cdot\mathbf{E}^{\rm cm,\parallel}_{\rm ind}(\mathbf{r},z)$$
$$= -Ze\iint\frac{d^2\mathbf{k}}{(2\pi)^2}\mathbf{v}\cdot\mathbf{E}^{\rm cm,\parallel}_{\rm ind}(\mathbf{k},b). \tag{20}$$

Using Eq. (17) in the last line of Eq. (20) and performing the angular integration over the direction of $\mathbf{k}$ with respect to $\mathbf{v}$, one may invoke parity properties of the functions $\sigma_{l,t}(k,\omega)$ to express the energy loss rate in a more familiar form involving integration over the frequency and the in-plane wavenumber [8],

$$\frac{dW}{dt} = \frac{2}{\pi}(Ze)^2\int_0^\infty\frac{dk}{k}\int_0^{kv}d\omega\,\omega\,{\rm e}^{-2|b|\alpha(k,\omega)}$$
$$\times\left\{\frac{\alpha(k,\omega)}{\sqrt{k^2v^2-\omega^2}}\Im\left[\frac{-1}{\epsilon_l(k,\omega)}\right]+\frac{\sqrt{k^2v^2-\omega^2}}{c^2\alpha(k,\omega)}\Im\left[\frac{1}{\epsilon_t(k,\omega)}\right]\right\}. \tag{21}$$

This result represents a modification of the formula (5.30) of Ref. [12], derived for the stopping power in the bulk of a solid, to the case of a charged particle moving parallel to a 2D target. From the expression in Eq. (21), it is obvious that any resonant modes in the conducting layer are given by the zeros of the 2D dielectric functions $\epsilon_{l,t}(k,\omega)$ in the (ω,k) plane. Those modes may be excited by the externally moving charged particle if their dispersion relations (in the limit of vanishing damping) traverse the boundary of the region $0 < \omega \leqslant kv$. Clearly, the two terms within the curly brackets in Eq. (21) represent contributions to the energy loss of the external charged particle resulting from the longitudinal and transverse polarizations of the electron gas in the conducting layer.

In the non-retarded limit, one lets $c \to \infty$ and hence $\alpha(k,\omega) \to k$ in Eq. (21), so that only the longitudinal contribution survives, giving the familiar expression for the energy loss rate [8,21–23]

$$\left.\frac{dW}{dt}\right|_{\rm nr} = \frac{2}{\pi}(Ze)^2\int_0^\infty dk\int_0^{kv}d\omega\,\frac{\omega}{\sqrt{k^2v^2-\omega^2}}{\rm e}^{-2|b|k}\Im\left[\frac{-1}{\epsilon_{\rm nr}(k,\omega)}\right], \tag{22}$$

with the usual definition of dielectric function for a 2D electron gas in the non-retarded limit,

$$\epsilon_{\rm nr}(k,\omega) = 1 + 2\pi i\frac{k}{\omega}\sigma_l(k,\omega). \tag{23}$$

3. Results and discussion

While the formalism developed in the previous section can be directly applied to any isotropic 2D material with tensorial in-plane conductivity, we limit our focus on doped graphene, where low-energy electron excitations within and between its π electron bands give rise to the Dirac plasmon, with an appealing property of tunability by changing the doping density of charge carriers in graphene, n, by using external gates [24]. Calculations of the conductivity of graphene using the Dirac cone approximation for its π electron bands [17,18], as well as the *ab initio* calculations based on all graphene bands [15], show that the longitudinal and transverse conductivities, $\sigma_{l,t}(\mathbf{k},\omega)$, exhibit rather different behaviors when the dependence on the wavevector $\mathbf{k}$ is included in those functions. On the other hand, applications of the DPP in Nanophotonics involve rather low frequencies, ranging from THz to mid-IR [24], so that it is safe to consider conductivities in the optical limit by letting $k \to 0$, in which case one finds that $\sigma_l(0,\omega) = \sigma_t(0,\omega) = \sigma(\omega)$ [17,18,16].

The dispersion relation for the DPP is readily deduced from zeros of the longitudinal dielectric function, $\epsilon_l(k,\omega) = 0$, by using a simple Drude model for conductivity in Eq. (18). This model describes *intraband* electron excitations in doped graphene in the optical limit, and is given at zero temperature by

$$\sigma_{\rm intra}(\omega) = i\frac{v_B}{\pi}\frac{\omega_F}{\omega+i\gamma}, \tag{24}$$

where $v_B = e^2/\hbar \approx c/137$ is the Bohr velocity, $\omega_F = \varepsilon_F/\hbar = v_F k_F$ is the frequency related to the Fermi energy ε_F in graphene, with $v_F \approx c/300$ being the Fermi speed in graphene and $k_F = \sqrt{\pi|n|}$ its Fermi wavenumber, whereas γ is the damping rate [25]. The range of validity of the Drude model in Eq. (24) is limited to frequencies satisfying the relations $kv_F \ll \omega \ll \omega_F$.

On the other hand, a collective mode due to transverse polarization of graphene has proven to be more elusive. Its existence was predicted theoretically by including *interband* electron transitions between the π electron bands in graphene, which may be described in the optical limit by a contribution to the conductivity, given at zero temperature and with zero damping by [16]

$$\sigma_{\rm inter}(\omega) = \frac{v_B}{4}\left[\Theta(\omega-2\omega_F)+\frac{i}{\pi}\ln\left|\frac{\omega-2\omega_F}{\omega+2\omega_F}\right|\right], \tag{25}$$

with Θ being the Heaviside unit step function. Combining the Drude and the interband contributions, Eqs. (24) and (25), gives a conductivity model $\sigma(\omega) = \sigma_{\rm intra}(\omega) + \sigma_{\rm inter}(\omega)$, which relaxes the requirement $\omega \ll \omega_F$. Using this model in Eq. (19) gives a condition for the

transverse plasmon polariton (TPP) from zeros of the transverse dielectric function, $\epsilon_t(k,\omega) = 0$. It was found that the dispersion of such a collective mode is pinned at the light line, $\omega = ck$, and would only be observable in a narrow range of frequencies close to $2\omega_F$ [16]. Since excitation of such a mode by an external charge moving parallel to graphene would require that the resonance condition is satisfied, $\omega = kv$, it appears that only ultrarelativistic particles with $v \to c$ would be capable of exciting the TPP in doped graphene placed in vacuum. While this indicates that the so-called relativistic density effect (see Section 5.6.4 in Ref. [12]) is possibly much weaker in graphene than in a solid target, a further detailed analysis of the TPP contribution in Eq. (21) is warranted, but is left for future work.

Therefore, we shall only study here energy loss of the external charged particle due to excitation of the DPP in doped graphene in the optical limit. Limiting our consideration to frequencies $\omega \ll \omega_F$ and taking the limit of zero damping, $\gamma \to 0^+$, in Eq. (24), one can show that the contribution of the transverse polarization in Eq. (21) vanishes, whereas the contribution of the longitudinal polarization may be well described by using just the Drude conductivity, Eq. (24), in Eq. (18), provided that the external charged particle is sufficiently fast.

To facilitate the computations, it is useful to introduce the reduced wavenumber and reduced frequency, $\overline{k} = k/k_c$ and $\overline{\omega} = \omega/\omega_c$, respectively, where $k_c = v_B v_F k_F/c^2$ and $\omega_c = ck_c = v_B v_F k_F/c$ [10]. We note that, using $|n| = 10^{13}$ cm^{-2} as typical doping density of graphene, the characteristic wavenumber attains the value $k_c \approx 1.36 \times 10^{-5}$ nm^{-1}, whereas the corresponding characteristic frequency yields $\hbar\omega_c \approx 2.69$ meV or $\nu_c = \omega_c/(2\pi) \approx 0.65$ THz. Using the reduced quantities, the conditions validating the Drude model may be written as $\frac{v_F}{c}\overline{k} \ll \overline{\omega} \ll \frac{c}{v_B}$.

By taking the limit of zero damping in Eq. (24), one can further show that the loss function $\Im[-1/\epsilon_l(k,\omega)]$ in Eq. (21) yields a Dirac's delta function that is peaked at the dispersion curve of the DPP, given in the reduced form by $\overline{\omega} = \sqrt{2(-1+\sqrt{1+\overline{k}^2})}$. Note that, in the non-retarded limit, this dispersion is reduced to $\overline{\omega} = \sqrt{2\overline{k}}$. Moreover, the resonance condition for exciting the DPP by a particle moving with the reduced speed $\beta = v/c$ may be written as $\overline{\omega} = \beta\overline{k}$, which crosses the DPP dispersion curve in a fully retarded limit at the reduced wavenumber $\overline{k}_r = \frac{2}{\beta}\sqrt{\beta^{-2}-1}$. It may be then shown that the pair of values $\overline{k}_r$ and $\overline{\omega}_r = \beta\overline{k}_r$ may be chosen so that the conditions validating the Drude model, are fulfilled when the speed of the external charged particle is $v \gg v_B$, or $\beta \gtrsim 0.1$.

In Fig. 1 we show both the retarded and non-retarded dispersion relations in the reduced units. One notices significant differences, where the retarded dispersion is placed below the light line for all wavenumbers, whereas the non-retarded dispersion lies above the light line for $0 < \overline{k} < 2$. Similarly, considering the resonance line for a particle with $v = 0.5c$, one sees that its intersections with the retarded and non-retarded dispersions occur at $\overline{k} \approx 7$ and $\overline{k} \approx 8$, respectively.

Next, taking advantage of the Dirac's delta function that results from the loss function $\Im[-1/\epsilon_l(k,\omega)]$ in Eq. (21), and introducing the auxiliary variable $y = (vk/\omega)^2 \equiv (\beta\overline{k}/\overline{\omega})^2$, one can write the final expression for the energy loss rate to the DPP excitation as

$$\frac{dW}{dt} = \frac{R}{\beta^3}\int_1^\infty dy\,\frac{(y-\beta^2)^{3/2}}{y\sqrt{y-1}}\exp\left[-4\frac{\overline{b}}{\beta^2}(y-\beta^2)\right], \tag{26}$$

where $R = (2Zek_c)^2 c \approx 3.2 \times 10^8$ eV/s $\approx 5.1 \times 10^{-11}$ W, and $\overline{b} = |b|k_c$ is the reduced distance. Notice that the value $\overline{b} = 1$ corresponds to a rather large physical distance of $|b| \approx 73.5$ μm.

To obtain the non-retarded result for energy loss, one needs to transform the expression that appears twice in the parentheses in Eq. (26) according to $(y-\beta^2) \to y$ giving

$$\left.\frac{dW}{dt}\right|_{\rm nr} = \widetilde{R}\int_1^\infty dy\,\sqrt{\frac{y}{y-1}}\exp(-4\widetilde{b}y) = \frac{\widetilde{R}}{2}e^{-2\widetilde{b}}[K_0(2\widetilde{b}) + K_1(2\widetilde{b})], \tag{27}$$

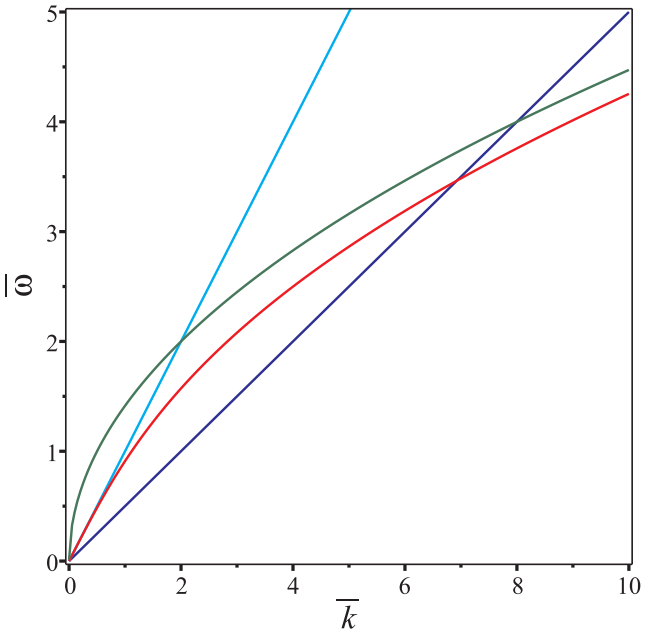

Fig. 1. Dispersion relations in reduced variables $\overline{\omega} = \omega/\omega_c$ and $\overline{k} = k/k_c$. Red: Dirac plasmon polariton (including retardation), $\overline{\omega} = \sqrt{2(-1+\sqrt{1+\overline{k}^2})}$. Green: Dirac plasmon (non-retarded limit), . Blue: resonance line, $\overline{\omega} = \beta\overline{k}$, for external charge with the reduced speed $\beta = v/c = 0.5$. Cyan: light line, $\overline{\omega} = \overline{k}$. (For interpretation of the references to colour in this figure legend, the reader is referred to the web version of this article.)

where $\widetilde{R} \equiv R/\beta^3 = (2Zek_F v_F v_B)^2/v^3$ and $\widetilde{b} \equiv \overline{b}/\beta^2 = |b|k_F v_F v_B/v^2$, whereas K_0 and K_1 are modified Bessel functions of the second kind.

Using the expressions in Eqs. (26) and (27), we evaluate the corresponding energy loss rates and show them in Fig. 2 as a function of the reduced distance $\overline{b}$ (for several reduced speeds β) and in Fig. 3 as a function of the reduced speed (for several reduced distances). One notices in Fig. 2 that the retardation effects increase with increasing distance and increasing speed, as expected. It is somewhat surprising that, at larger speeds, the retarded energy loss tends to exceed the non-retarded loss at large distances, but this trend is reversed for intermediate and shorter distances.

Given the strong decrease of the energy loss rate with distance, we have multiplied each curve in Fig. 3 by a suitable factor, so that all the retarded curves in that figure have the same maximum value, with a position that depends on the reduced speed. One notices that the positions of these maxima increase with the reduced distance, as expected. Moreover, as the distance increases, one also notices increasing differences between the retarded and non-retarded energy loss rates, such that the non-retarded energy losses are larger than the retarded losses at sufficiently large speeds, whereas this trend is reversed at lower speeds.

Both Figs. 2 and 3 exhibit an interesting dependence of the ratio of the retarded to the non-retarded energy loss rates as a function of the reduced particle speed in a range $0.2 \lesssim \beta < 1$ and the reduced distance in a range $0.01 \lesssim \overline{b} \lesssim 1$. This behavior may be qualitatively analyzed by applying the Mean-Value Theorem to the factor $(y-\beta^2)^{3/2}$ in the integral in Eq. (26), giving

$$\frac{dW}{dt} = e^{4\overline{b}}\left(1-\frac{\beta^2}{y_*}\right)^{3/2}\left.\frac{dW}{dt}\right|_{\rm nr}, \tag{28}$$

where $y_* \gtrsim 1$. This expression shows that the ratio of the retarded to the non-retarded energy loss rates may take values <1 for increasing β and decreasing $\overline{b}$, and >1 for increasing $\overline{b}$ and decreasing β. However, from both Figs. 2 and 3, one observes that at distances shorter than about $\overline{b} = 10^{-3}$, i.e., for $|b| \lesssim 73.5$ nm, there are practically no differences between the retarded and non-retarded energy loss rates in the full range

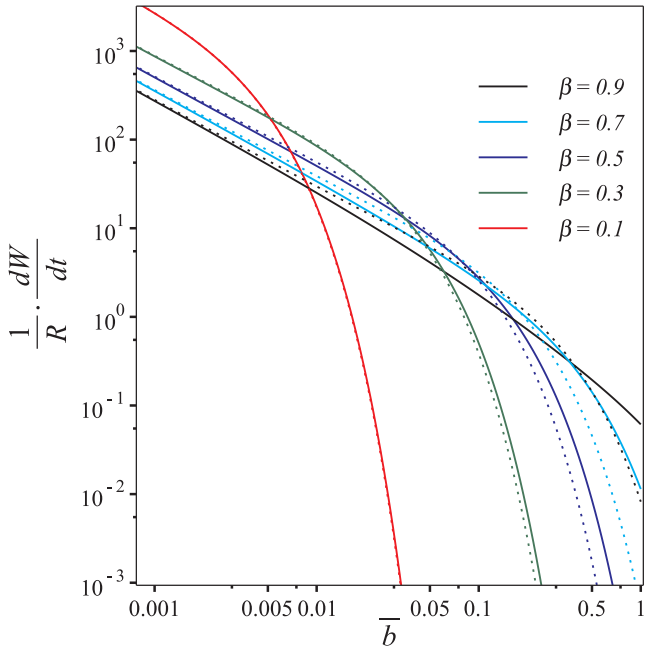

Fig. 2. Solid lines show the retarded, and the dotted lines show the non-retarded energy loss rate $\frac{dW}{dt}$ divided by the factor R as a function of the reduced distance $\bar{b} = |b|k_c$ of external charged particle with $Z = 1$ that moves parallel to doped graphene at the reduced speed $\beta = v/c$, which takes values $\beta = 0.1$ (red curves), $\beta = 0.3$ (green curves), $\beta = 0.5$ (blue curves), $\beta = 0.7$ (cyan curves) and $\beta = 0.9$ (black curves). (For interpretation of the references to colour in this figure legend, the reader is referred to the web version of this article.)

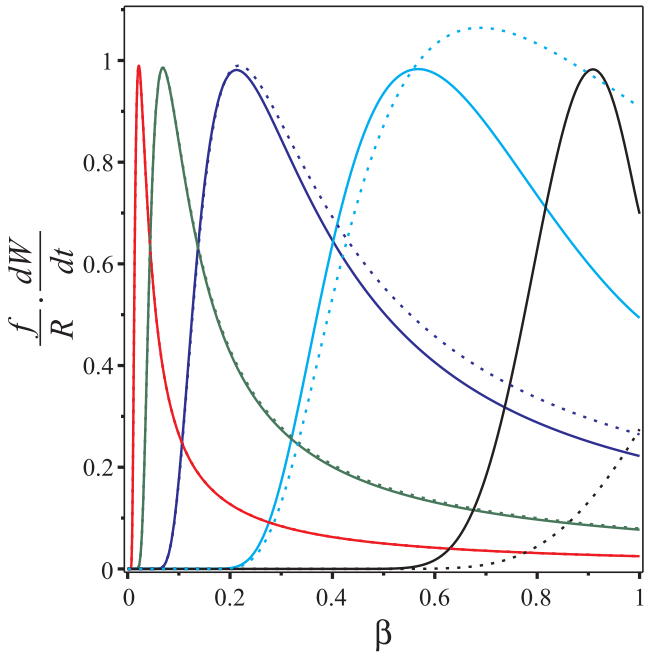

Fig. 3. Solid lines show the retarded, and the dotted lines show the non-retarded energy loss rate $\frac{dW}{dt}$ multiplied by the factor $\frac{f}{R}$ as a function of the reduced speed $\beta = v/c$ of external charged particle with $Z = 1$ that moves parallel to doped graphene at the reduced distance $\bar{b} = |b|k_c$, which takes values $\bar{b} = 10^{-4}$ (red curves with $f = 10^{-5}$), $\bar{b} = 10^{-3}$ (green curves with $f = 3.15 \times 10^{-4}$), $\bar{b} = 10^{-2}$ (blue curves with $f = 10^{-2}$), $\bar{b} = 10^{-1}$ (cyan curves with $f = 0.34$) and $\bar{b} = 1$ (black curves with $f = 16$). (For interpretation of the references to colour in this figure legend, the reader is referred to the web version of this article.)

of the incident particle speeds.

It may be worthwhile mentioning that, by attaching a semiclassical interpretation to the expressions for the energy loss rate given in Eqs. (21) and (22), one can calculate the corresponding inverse inelastic lifetimes of the external charged particle, Γ and $\Gamma_{\rm nr}$, respectively. This is achieved by simply replacing the factor ω in the integrands in those equations with a factor $1/\hbar$ [21]. Furthermore, by taking the limit of zero damping in the loss function $\Im[-1/\epsilon_l(k,\omega)]$, the thus obtained expressions for Γ and $\Gamma_{\rm nr}$ yield the rates of excitation of the DPP in doped graphene by the external charged particle in a fully retarded and non-retarded regimes, respectively. It is interesting that, following the same procedure as that used in deriving Eqs. (26) and (27), both those rates can be evaluated in terms of elementary functions as

$$\Gamma = \frac{Q}{\beta} e^{4\bar{b}} \left[\frac{1}{\sqrt{\bar{b}}} e^{-4\frac{\bar{b}}{\beta^2}} - 2\sqrt{\pi}\beta \,\mathrm{erfc}\left(\frac{2}{\beta}\sqrt{\bar{b}}\right)\right], \tag{29}$$

where $Q = \sqrt{\pi}\omega_F \left(\frac{v_B}{c}\right)^2 \approx 53$ GHz, and erfc is the complementary error function, and

$$\Gamma_{\rm nr} = \frac{\widetilde{Q}}{\sqrt{\widetilde{b}}} e^{-4\widetilde{b}}, \tag{30}$$

where $\widetilde{Q} = Q/\beta^2$ and $\widetilde{b} = \bar{b}/\beta^2$. A simple analysis of Eqs. (29) and (30) shows that the ratio of the retarded and non-retarded excitation rates for the DPP, $\Gamma/\Gamma_{\rm nr}$, exhibits a similar dependence on the reduced particle speed β and the reduced distance $\bar{b}$ as the ratio of the energy loss rates, discussed above.

4. Concluding remarks

We have presented a fully relativistic formulation for the energy loss rate of a charged particle moving parallel to a sheet containing two-dimensional electron gas, and applied it to a single doped graphene layer. While our formulation of the problem allows for different longitudinal and transverse in-plane conductivities of graphene, limiting our attention to the THz range of frequencies allowed us to work in the optical limit, where those conductivities are well approximated by a Drude model. Taking this model in the limit of zero damping allowed us to evaluate the energy loss rates due to excitation of the Dirac plasmon polariton in doped graphene by a charged particle that moves at speeds in excess of about one tenth of the speed of light.

We have observed that the retardation effects are important when the incident particle speed and its distance from graphene both increase, as expected. However, there are some interesting, non-monotonous relations between the values of the retarded and non-retarded energy loss rates. Namely, for a given particle speed, the retarded loss rate is greater than the non-retarded rate at large distances, but this trend is reversed at shorter distances, whereas for a given distance, the non-retarded loss rate is greater than the retarded rate at high speeds, but this trend is reversed at lower speeds. On the other hand, using the parameters relevant for the Dirac plasmon in a typically doped graphene layer, we have found no significant retardation effects for distances of the charged particle trajectory up to ~ 100 nm. Given that in most experiments using aloof scattering of electrons the distance of closest approach does not reach so large values, we may conclude that non-relativistic treatment would be valid for studying Dirac plasmons in graphene.

Acknowledgments

Z.L.M. acknowledges support from the Natural Sciences and Engineering Research Council of Canada (Grant No. 2016-03689). Argentinean team acknowledges the financial support from CONICET (PIP 11220120100374) and ANPCyT (PICT 2012–1136) from Argentina.

References

[1] F. Xia, H. Wang, D. Xiao, M. Dubey, A. Ramasubramaniam, Nat Photonics 8 (2014) 899, http://dx.doi.org/10.1038/nphoton.2014.271.
[2] F.J. Garcia de Abajo, ACS Photonics 1 (2014) 135, http://dx.doi.org/10.1021/ph400147y.
[3] S. Xiao, X. Zhu, B.-H. Li, N.A. Mortensen, Front. Phys. 11 (2016) 117801, http://dx.doi.org/10.1007/s11467-016-0551-z.
[4] T. Zhan, D. Han, X. Hu, X. Liu, S.-T. Chui, J. Zi, Phys. Rev. B 89 (2014) 245434 http://link.aps.org/doi/10.1103/PhysRevB.89.245434.
[5] S. Liu, C. Zhang, M. Hu, X. Chen, P. Zhang, G. Sen, T. Zhao, R. Zhong, Appl. Phys. Lett. 104 (2014) 201104.
[6] K.-C. Zhang, X.-X. Chen, C.-J. Sheng, K. Ooi, L. Ang, X.-S. Yuan, Opt. Express 25 (2017) 20477.
[7] F.H.L. Koppens, D.E. Chang, F.J. García de Abajo, Nano Lett. 11 (2011) 3370, http://dx.doi.org/10.1021/nl201771h.
[8] K.F. Allison, D. Borka, I. Radović, L. Hadžievski, Z.L. Mišković, Phys. Rev. B 80 (2009) 195405 https://link.aps.org/doi/10.1103/PhysRevB.80.195405.
[9] T. Markovic, I. Radovic, D. Borka, Z.L. Miskovic, Plasmonics 10 (2015) 1741–1749.
[10] Z.L. Mišković, S. Segui, J.L. Gervasoni, N.R. Arista, Phys. Rev. B 94 (2016) 125414 http://link.aps.org/doi/10.1103/PhysRevB.94.125414.
[11] K. Akbari, Z.L. Mišković, S. Segui, J.L. Gervasoni, N.R. Arista, ACS Photonics 4 (1980) 2017, http://dx.doi.org/10.1021/acsphotonics.7b00344.
[12] P. Sigmund,, Particle Penetration and Radiation Effects, Volume 1: General Aspects and Stopping of Swift Point Charges, Springer, New York, 2006.
[13] R. Garcia-Molina, A. Gras-Marti, A. Howie, R.H. Ritchie, J. Phys. C: Solid State Phys. 18 (1985) 5335.
[14] A. Rivacoba, N. Zabala, New J. Phys. 16 (2014) 073048.
[15] D. Novko, M. Šunjić, V. Despoja, Phys. Rev. B 93 (2016) 125413 https://link.aps.org/doi/10.1103/PhysRevB.93.125413.
[16] S.A. Mikhailov, K. Ziegler, Phys. Rev. Lett 99 (2007) 16803 https://link.aps.org/doi/10.1103/PhysRevLett. 99.016803.
[17] A. Principi, M. Polini, G. Vignale, Phys. Rev. B 80 (2009) 75418 https://link.aps.org/doi/10.1103/PhysRevB.80.075418.
[18] T. Stauber, G. Gómez-Santos, Phys. Rev. B 82 (2010) 155412 https://link.aps.org/doi/10.1103/PhysRevB.82.155412.
[19] J.D. Jackson, Classical Electrodynamics, third ed., Wiley, New York, 1999 http://cdsweb.cern.ch/record/490457.
[20] J.A. Stratton, Electromagnetic Theory, McGraw-Hill, New York, 1941.
[21] R. Núñez, P.M. Echenique, R.H. Ritchie, J. Phys. C: Solid St. Phys. 13 (1980) 4229.
[22] M. Alducin, V.M. Silkin, J.I. Juaristi, Nucl. Instrum. Methods Phys. Res. B 256 (2007) 383.
[23] V.M. Silkin, M. Alducin, J.I. Juaristi, E.V. Chulkov, P.M. Echenique, J. Phys.: Condens. Matter 20 (2008) 304209.
[24] Z. Fei, A.S. Rodin, G.O. Andreev, W. Bao, A.S. McLeod, M. Wagner, L.M. Zhang, Z. Zhao, M. Thiemens, G. Dominguez, M.M. Fogler, A.H.C. Neto, C.N. Lau, F. Keilmann, D.N. Basov, Nature 487 (2012) 82, http://dx.doi.org/10.1038/nature11253 http://www.nature.com/nature/journal/v487/n7405/abs/nature11253.html#supplementary-information.
[25] S. Das Sarma, S. Adam, E.H. Hwang, E. Rossi, Rev. Mod. Phys. 83 (2011) 407 http://link.aps.org/doi/10.1103/RevModPhys.83.407.